J. Phys. B: At. Mol. Opt. Phys. **46** (2013) 065302 (11pp) doi:10.1088/0953-4075/46/6/065302

Scattering of atomic dark–bright solitons from narrow impurities

A Álvarez[1], J Cuevas[2], F R Romero[1], C Hamner[3], J J Chang[3], P Engels[3], P G Kevrekidis[4] and D J Frantzeskakis[5]

[1] Grupo de Física No Lineal, Universidad de Sevilla, Área de Física Teórica, Facultad de Física, Avda. Reina Mercedes, s/n, E-41012 Sevilla, Spain
[2] Grupo de Física No Lineal, Universidad de Sevilla, Departamento de Física Aplicada I, Escuela Politécnica Superior, C/ Virgen de África, 7, E-41011 Sevilla, Spain
[3] Department of Physics and Astronomy, Washington State University, Pullman, WA 99164, USA
[4] Department of Mathematics and Statistics, University of Massachusetts, Amherst, MA 01003-4515, USA
[5] Department of Physics, University of Athens, Panepistimiopolis, Zografos, Athens 157 84, Greece

E-mail: kevrekid@math.umass.edu

Received 24 October 2012, in final form 29 December 2012
Published 1 March 2013
Online at stacks.iop.org/JPhysB/46/065302

Abstract
In this work, we examine the collision of an atomic dark–bright soliton, in a two-component Bose–Einstein condensate, with a Gaussian barrier or well. Our study has both an experimental component and a theoretical/computational one. First, we present the results of an experiment, illustrating the classical particle phenomenology (transmission or reflection) in the case of an equal barrier in both components. Then, motivated by the experimental observations, we perform systematic simulations considering not only the case of equal heights of a barrier (or a well), but also the considerably more complex setting, where the potential affects only one of the two components. We systematically classify the ensuing cases within a two-parameter diagram of potential amplitudes in the two components, and provide intuitive explanations for the resulting observations, as well as of their variations as the strength of the potential changes.

(Some figures may appear in colour only in the online journal)

1. Introduction

Atomic Bose–Einstein condensates (BECs) [1, 2] provide an ideal platform for the study of nonlinear phenomena at the mesoscopic scale (see, e.g., the reviews [3–6]). In this context, of particular interest are multi-component BECs, which—in their simplest version—are composed of two different hyperfine atomic levels of the same atom (e.g., ^{87}Rb [7, 8]). In such systems, a rich variety of structures can be observed, which can *not* arise in single-component BECs. Regarding macroscopic nonlinear excitations of multi-component BECs, a distinctive feature of interest involves the potential formation of dark–bright (DB) solitons. This type of vector soliton consists of a dark soliton in one component coupled to a bright soliton in the second component. These solitons in repulsive homogeneous BECs are usually referred to as 'symbiotic' solitons, with this characterization stemming from the fact that the bright component cannot be supported in a stand-alone fashion (it is only supported as such in attractive BECs [9, 10]; see also the review [5]), and is only sustained because of the presence of its dark counterpart, which acts as an effective external trapping potential. We highlight here the fact that we refer to homogeneous BECs, as in the presence of external potentials, such as optical lattices, bright (gap) solitons can be sustained in repulsive BECs [11], but are critically shaped by the form of the potential.

DB solitons have been studied extensively in different settings in a large number of theoretical works (see, e.g., [12–21]), while they have also been observed in experiments, both in two-component ^{87}Rb BECs [22–27] and in nonlinear optics [28–31]. In the BEC context, these experimental studies have chiefly involved the dynamics of a single DB soliton in a trap [22, 24], the generation of multiple DB solitons in a counterflow experiment [23], the study of their interactions [25], as well as the creation of SU(2)-rotated DB solitons, in the form of beating dark–dark solitons [26, 27].

On the other hand, the fundamental problem of the interaction of solitons with localized impurities has been considered both in nonlinear wave theory [32] and solid state physics [33]. The interaction of either bright or dark solitons with δ-like impurities has been investigated in the framework of the nonlinear Schrödinger (NLS) equation (see, e.g., [34–38]). Relevant studies in the physics of atomic BECs have also appeared some time ago (see, e.g., [39–41]). Among these works, [39] considered a dark soliton as perturbed by a defect (both the steady state, and the associated dynamical problem), while [40] examined the collision of a moving dark soliton with a defect and captured also the leading-order effect of produced radiation. Recent studies have chiefly been concerned with bright solitons both in the setting of potential wells [42, 43] (examining resonances that can arise therein), and in that of barriers [44, 45].

Most of the above works have been restricted to the mean-field description of the NLS equation. Nevertheless, the potential role of quantum fluctuations in such interactions (especially for smaller atom numbers or narrower barriers) has been illustrated; see e.g. [45]. Generally, the examination of quantum effects in soliton–barrier [46, 47] and even soliton–soliton [48] interactions is a subject of increasing interest over the past few years. It has been argued, in particular, that the scattering of a bright solitary wave in an attractive BEC from a barrier potential leads to the formation of a quantum superposition state of two distinct wave packets travelling through real space [46]. The full quantum mechanical scattering problem for short-range potentials and at low energy was considered in [47] and error bounds on the scattering coefficients were derived. Finally, in [48] it was argued that initially uncorrelated quantum solitons lead to entanglement, upon their pair-wise interaction.

Finally, as concerns two-component systems, the work of [49] has also mostly focused on bright soliton–barrier interactions at the NLS level, yet is the first one to touch upon DB soliton interactions with a barrier acting on the bright soliton only. In this context, localized impurities can be created as focused far-detuned laser beams and have already been used in experiments with dark solitons [50, 51]; we also note very recent experiments with matter–wave bright solitons of ^{7}Li [52] and ^{85}Rb [53] atoms and localized barriers. However, such soliton–defect interactions are far less well explored in the case of the multi-component setting (see, e.g., [20] where the statics of DB solitons was studied in the presence of δ-like impurities). It is the aim of this work to address this problem and study, in particular, the scattering of atomic DB solitons at narrow impurities. Nevertheless, it should be noted that here we will restrict our considerations to the mean-field level. It would be an interesting problem for further study to examine how quantum mechanical effects modify the phenomenology presented herein.

Our presentation will be structured as follows. In section 2, we present the relevant prototypical model setup in the form of two coupled Gross–Pitaevskii (GP) equations describing the dynamics of a binary BEC with repulsive interactions; DB solitons for this model are presented as well. We also present results of a prototypical experiment where the scattering of DB solitons at a barrier—which is present (and equal) in both atomic components—is studied; this experiment provides the motivation for a more systematic theoretical study which is presented in the next section. In particular, in section 3, we numerically explore the dynamics of single DB solitons in a harmonic trap. The simpler scenario that is studied refers to the case where the impurity is equal in the two components—as in the case of the experiment; we find that a particle-based phenomenology is sufficient to capture the main characteristics here. On the other hand, we identify a far more significant wealth of possibilities in the setting where the barrier (or well) is applicable only in one of the two components. We present a systematic study within the plane of the barrier or well amplitudes for the two components, providing intuitive explanations (on the basis of effective potentials), wherever possible, for the observed phenomenology. Finally, in section 4, we summarize our findings and present our conclusions, as well as a number of directions for potential future studies.

2. Model and experimental motivation

2.1. Gross–Pitaevskii equations and dark–bright solitons

We consider a two-component BEC composed of two different hyperfine states of the same alkali isotope. If this binary condensate is confined in a highly anisotropic trap (with longitudinal and transverse trapping frequencies $\omega_x \ll \omega_\perp$), then the mean-field dynamics of the BEC can be described by the following system of two coupled GP equations [1, 2]:

$$\mathrm{i}\hbar\partial_t\psi_j = \left(-\frac{\hbar^2}{2m}\partial_x^2\psi_j + V_j(x) - \mu_j + \sum_{k=1}^{2} g_{jk}|\psi_k|^2\right)\psi_j, \tag{1}$$

where $\psi_j(x,t)$ $(j=1,2)$ are the macroscopic wave functions of the two components normalized to the numbers of atoms $N_j = \int_{-\infty}^{+\infty}|\psi_j|^2\,\mathrm{d}x$, m is the atomic mass, μ_j are the chemical potentials, $g_{jk} = 2\hbar\omega_\perp a_{jk}$ are the effective 1D coupling constants (a_{jk} are the s-wave scattering lengths), while $V_j(x)$ denote the external trapping potentials for each species. In our considerations below, we will assume that the component 1 (2) supports a dark (bright) soliton; additionally, we will assume that both components are confined by the usual harmonic trap, namely $V_H(x) = (1/2)m\omega_x^2x^2$, while—for each component—an additional localized 'impurity' potential, which can be generated by off-resonant Gaussian laser beams, is also present. Thus, the external potentials $V_j(x)$ for each of the two components are described as

$$V_1(x) = V_H + E_d\exp\left(-\frac{2x^2}{\epsilon_d^2}\right),$$
$$V_2(x) = V_H + E_b\exp\left(-\frac{2x^2}{\epsilon_b^2}\right), \tag{2}$$

where the parameters E_d, E_b and ϵ_d, ϵ_b set, respectively, the amplitudes and widths of the impurities in each component. Notice that for a blue- or red-detuned laser beam, the impurity

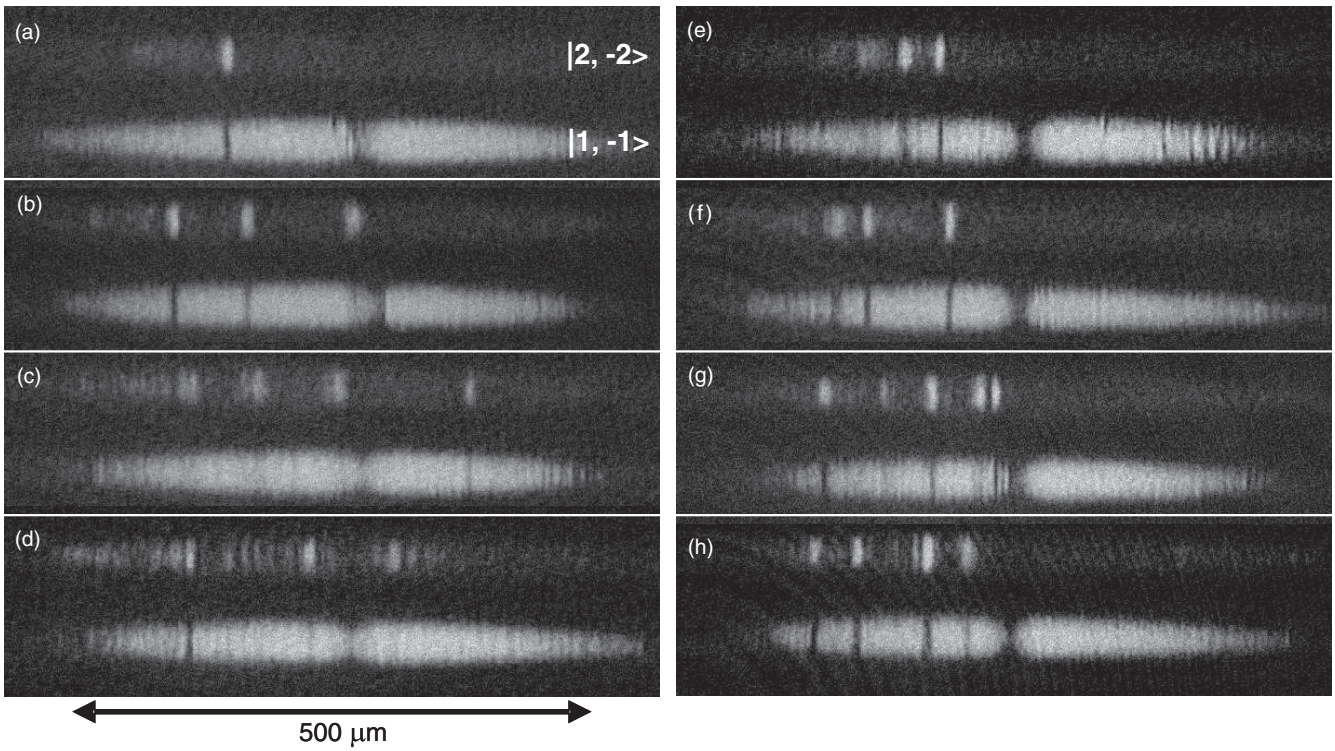

Figure 1. Experimental images of soliton–barrier interaction. (a)–(d) The peak barrier potential is $0.56 \cdot \mu_{\rm BEC}$. The in-trap evolution times after generation of the solitons are (a) 250 ms, (b) 500 ms, (c) 750 ms, (d) 1000 ms. (e)–(h) Similar to (a)–(d) but for a peak barrier potential of $1.11 \cdot \mu_{\rm BEC}$ and evolution times (e) 300 ms, (f) 600 ms, (g) 700 ms, (h) 900 ms. In all cases the chemical potential of the BEC, $\mu_{\rm BEC}$, is approximately 36 nK (about 750 Hz).

potentials can either *repel* ($E_{d,b} > 0$) or *attract* ($E_{d,b} < 0$) the atoms of the respective component of the condensate.

We now cast equation (1) into a dimensionless form as follows: measuring the densities $|\psi_j|^2$, length, time and energy in units of $2a_{11}$, $a_\perp = \sqrt{\hbar/(m\omega_\perp)}$, $\omega_\perp^{-1}$ and $\hbar\omega_\perp$, respectively, the equations in (1) are reduced to the form:

$$\mathrm{i}\partial_t u = -\tfrac{1}{2}\partial_x^2 u + V_1(x)u + (|u|^2 + \tilde{g}_{12}|v|^2 - \mu_1)u, \tag{3}$$

$$\mathrm{i}\partial_t v = -\tfrac{1}{2}\partial_x^2 v + V_2(x)v + (\tilde{g}_{12}|u|^2 + \tilde{g}_{22}|v|^2 - \mu_2)v. \tag{4}$$

In equations (3)–(4), the wave functions u and v correspond to ψ_1 and ψ_2 respectively, the normalized nonlinearity coefficients are given by $\tilde{g}_{j2} = g_{j2}/g_{11}$, while the normalized harmonic trap potential (incorporated in $V_1(x)$ and $V_2(x)$ as discussed above) is now given by $V_H(x) = (1/2)\Omega^2 x^2$, where $\Omega = \omega_x/\omega_\perp$.

Notice that in the GP equations (3)–(4) the number of atoms $N_{D,B}$ of each component is conserved; in fact, $N_{D,B}$ are given by $N_{D,B} = (a_\perp/2a_{11})\tilde{N}_{D,B}$, where $\tilde{N}_D = \int_{-\infty}^{\infty} |u(x)|^2\,\mathrm{d}x$ and $\tilde{N}_B = \int_{-\infty}^{\infty} |v(x)|^2\,\mathrm{d}x$ are the respective integrals of motion of the normalized GP equations (3)–(4).

As mentioned above, in the physically relevant setting of ^{87}Rb, the scattering lengths characterizing the intra- and inter-component atomic collisions are almost equal; thus, to a first approximation, one may assume that $\tilde{g}_{12} = \tilde{g}_{22} \approx 1$, which means that the system of equations (3)–(4) is of the Manakov type [54]; in this case, the system is integrable in the absence of the external potentials $V_{1,2}(x)$ and admits exact analytical DB soliton solutions. Particularly, considering the boundary conditions $|u|^2 \to \mu_1$ and $|v|^2 \to 0$ as $|x| \to \infty$, equations (3)–(4) possess an exact analytical one-DB-soliton solution of the following form (see, e.g., [12]):

$$u_{\rm DB}(x,t) = \sqrt{\mu_1}\{\cos\phi \tanh\xi + \mathrm{i}\sin\phi\}, \tag{5}$$

$$v_{\rm DB}(x,t) = \eta \,\mathrm{sech}\xi \exp[\mathrm{i}kx + \mathrm{i}\theta(t)], \tag{6}$$

where $\xi = D(x - x_0(t))$, ϕ is the dark soliton's phase angle, $\cos\phi$ and η represent the amplitudes of the dark and bright solitons, and D and $x_0(t)$ are associated with the inverse width and the centre position of the DB soliton. Furthermore, $k = D\tan\phi = \text{const}$ and $\theta(t)$ are the wavenumber and phase of the bright soliton, respectively. The above parameters of the DB-soliton are connected through the equations: $D^2 = \mu_1\cos^2\phi - \eta^2$, $\dot{x}_0 = D\tan\phi$, and $\theta(t) = (1/2)(D^2 - k^2 + \mu_2 - \mu_1)t$, where $\dot{x}_0$ is the DB soliton velocity.

2.2. Experimental results

Having introduced our setup, we now proceed by presenting results of an experiment dealing with scattering of atomic DB solitons at barriers. In fact, the results that will be presented below, motivate the more detailed theoretical investigation of this work, but also illustrate the experimental tractability of this direction, and showcase prototypical results along this vein.

Our experimental results are summarized in figure 1. There, it is shown that, depending on the barrier height, DB solitons are either reflected by or transmitted through a repulsive barrier.

The experiment is conducted with a BEC of 4.5×10^5 atoms of ^{87}Rb confined in an optical dipole trap with trapping frequencies $\{\omega_{\text{axial}}, \omega_{\text{vertical}}, \omega_{\text{horizontal}}\} = 2\pi \times \{1.4, 120, 174\}$ Hz. The solitons are generated by transferring a small fraction of the atoms from the initial $|F, m_F\rangle = |1, -1\rangle$ hyperfine state to the $|2, -2\rangle$ state, and exploiting a counter-flow induced modulational instability [23] generated by a magnetic gradient along the axial direction. The number of solitons, as well as their initial positions, can in principle be controlled by adjusting experimental parameters, such as the number of atoms transferred into the second state, and the strength and duration of the magnetic gradient used to induce the counter-flow. Here, it is relevant to note that regardless of the number of the generated DB solitons (the data for figure 1 correspond to a case of multiple solitons), the basic particle-like nature of solitons is clearly demonstrated, as is explained in more detail below.

As shown in figure 1, DB solitons travelling to the right are generated in the left part of the BEC; the magnetic gradient is subsequently turned off, and the solitons continue to move towards the trap centre. The oscillations of individual solitons in a trap have been investigated in detail in [24]. For the present data, we additionally ramp on a repulsive barrier at the centre of the trap. The barrier is generated from a 660 nm laser beam with a narrow waist of approximately 18 μm in the direction of the BEC axis and has an aspect ratio of 4. For imaging, the two components of the BEC are vertically separated during a short free expansion time of 7 ms for the upper cloud and 8 ms for the lower cloud [23, 24]. For barrier depths larger than the chemical potential (cf figures 1(e)–(h)), we observe confinement of the DB solitons to the left half of the BEC. This is consistent with having two isolated BECs. For a barrier depth of approximately half the chemical potential (cf figures 1(a)–(d)) we observe solitons penetrating through the barrier; see, e.g., especially panel (c) in this setting. The dynamics observed here is a subset of the rich behaviour expected for soliton–barrier interactions. These dynamics can be extended to more exotic regimes, e.g., by the addition of a species selective barrier. The latter will be examined in more detail in our theoretical investigation below.

3. Numerical investigations

In our numerical simulations below, we will assume that the two-component BEC under consideration consists of two different hyperfine states of ^{87}Rb, namely the states $|1, -1\rangle$ and $|2, -2\rangle$ used in the experiment presented in the previous section (see also [22–27]). In this case, the scattering lengths take the values $a_{11} = 100.4a_0$, $a_{12} = 98.98a_0$ and $a_{22} = 98.98a_0$ (where a_0 is the Bohr radius); accordingly, the normalized nonlinearity coefficients in equations (3)–(4) take equal values: $\tilde{g}_{12} = \tilde{g}_{22} \approx 0.986$. Furthermore, we will assume that the trap frequencies are $\omega_\perp = 2\pi \times 116$ Hz and $\omega_z = 2\pi \times 1.3$ Hz, i.e. $\Omega \approx 0.0112$, and the number of atoms in each component are $N_D = 70\,000$ and $N_B = 1000$ resulting in a chemical potential of approximately 305 Hz for the total atom number. These values are similar to the respective ones used in experiments [22–27].

Concerning the parameters of the Gaussian impurity potential, the values of $E_{b,d}$ are taken in the interval $[-200, 200]$ Hz, and we fix the value $\epsilon_d = \epsilon_b = \epsilon = 3$ μm. Notice that we focus here on relatively narrow impurities, as for those we have explored the steady-state problem [20] and, as will be seen below, they already present a rich phenomenology. An examination of the effect of the width of the impurity will be deferred to a future study. Our principal aim in what follows is to study the scattering of solitons at the impurity potential. To do so, we displace the solitons from the trap centre, using the initial position value $x_0 = -40$ μm, which is sufficiently far from $x = 0$, so that the solitons do not overlap with the impurity. We then 'release' the solitons and observe their subsequent interaction with the Gaussian barrier, measuring the fraction and observing also the shape of the coherent atomic localized structures that are transmitted, reflected, and trapped at the potential. We will study, at first, the case $E_b = E_d$, as per our experimental results (cf subsection 3.1 below) and then the case where the impurity acts only on one component, i.e. either $E_d = 0, E_b \neq 0$ or $E_d \neq 0, E_b = 0$ (cf subsection 3.2 below).

At this point, it is relevant to present a sketch of a state diagram in the parameter space (E_b, E_d), as depicted in figure 2. The different regimes that appear after the collisions are illustrated by colours and they will be discussed below. Cases I ($E_d = E_b = E$), II ($E_d = 0, E_b > 0$) and III ($E_d = 0, E_b < 0$) correspond to the principal cases that we will examine in what follows; the capital letters A and B correspond, respectively, to a small and large value of the parameters in each region. In particular, we have taken $E = 10$ Hz ($E = 50$ Hz) in the IA (IB) case, $E_b = 10$ Hz ($E_b = 90$ Hz) in the IIA (IIB) case, and $E_b = -10$ Hz ($E_b = -90$ Hz) for the IIIA (IIIB) case. For each A and B case, we will illustrate contour plots of the densities of both components. Furthermore, in the case where $E_d = E_b = E$ where as we will see below the 'particle-like' picture is most relevant, we will also display an effective potential energy landscape encountered by the DB solitons. This amounts to computing the turning point, say x_1, of each of our initializations of the DB soliton at position x_0 (whose potential energy $V_H(x_0)$ can easily be evaluated in a parabolic trap). Then, $(x_1, V_H(x_0))$ is identified as a point in the effective potential energy surface.

3.1. Scattering of DB solitons from identical impurities

We start with the case where both impurities are identical, i.e. $E_d = E_b = E$, either repulsive ($E > 0$) or attractive ($E < 0$).

In the repulsive case of $E_d = E_b = E > 0$, the simulations reveal the existence of two different regimes. For sufficiently small values of the repulsive barrier E, the DB solitons are transmitted (transmission regime, coloured blue in region I of figure 2). For values of E bigger than a critical value, i.e. $E \gtrsim 20$ Hz (for solitons launched from $x_0 = 40$ μm) the DB solitons are reflected (reflection regime, coloured red in the same region I of figure 2). Thus, in this case, the solitons behave as classical particles: if they have potential energy (recall that the solitons start with zero kinetic energy) larger than the height of the barrier then they are transmitted through it, while they are reflected in the opposite case.

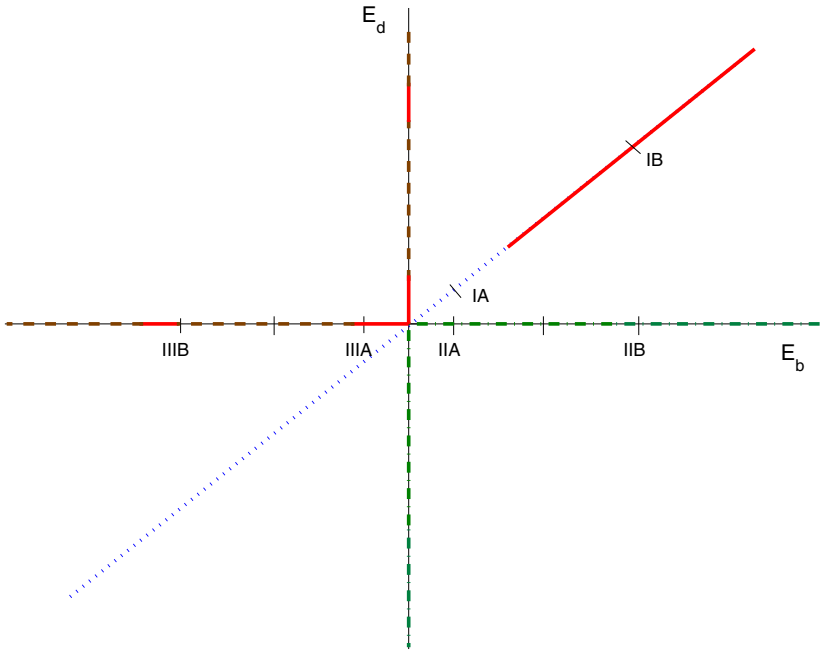

Figure 2. A theoretical state diagram in the parameter space (E_b, E_d). The four different regimes that appear after the collisions are illustrated by colours/line styles, as follows. Blue/dotted line: transmission regime; red/solid line: reflection regime; green/dash–dotted line: transmission-reflection regime; brown/dashed line: trapping-transmission-reflection regime. Points *A* and *B* correspond, respectively, to small and large values of the parameters in each region: I ($E_d = E_b = E$), II ($E_d = 0, E_b > 0$) and III ($E_d = 0, E_b < 0$).

This particle-like behaviour can be quantitatively described as follows. First, we consider the DB-soliton's potential energy difference ΔU caused by the defect, which can be defined as

$$\Delta U = U_{\rm def} - U_0, \tag{7}$$

with $U_{\rm def}$ (U_0) being the normalized potential energy of the DB soliton at the trap centre with(out) the defect:

$$U_{\rm def} = \frac{\int_{-\infty}^{\infty} {\rm d}x V_1(x)|u'(x)|^2}{\int_{-\infty}^{\infty} {\rm d}x\,|u'(x)|^2} + \frac{\int_{-\infty}^{\infty} {\rm d}x V_2(x)|v'(x)|^2}{\int_{-\infty}^{\infty} {\rm d}x\,|v'(x)|^2}, \tag{8}$$

$$U_0 = \frac{\int_{-\infty}^{\infty} {\rm d}x V_H(x)|u_0(x)|^2}{\int_{-\infty}^{\infty} {\rm d}x\,|u_0(x)|^2} + \frac{\int_{-\infty}^{\infty} {\rm d}x V_H(x)|v_0(x)|^2}{\int_{-\infty}^{\infty} {\rm d}x\,|v_0(x)|^2}. \tag{9}$$

In the above expressions, $\{u'(x), v'(x)\}$ and $\{u_0(x), v_0(x)\}$ denote, respectively, the DB solitons at the trap centre with and without the defect, as found numerically by means of a fixed point algorithm, using as an initial guess equations (5)–(6). Notice that the solutions with the prime are found by keeping fixed the chemical potentials $\mu_{1,2}$ of each component to those of the solution without defect.

Figure 3 shows the dependence of ΔU on $E_d = E_b$ (solid line in the figure), as well as its comparison with the maximum of the effective barrier height that the DB-soliton particle encounters at the defect (red circles in the figure). The latter quantity is found by means of numerical simulations, fixing the initial soliton location x_0 or, equivalently, of the potential energy of the soliton, i.e. $(1/2)\Omega^2 x_0^2$, and varying $E_d = E_b$ in order to determine the critical value which separates the reflection and transmission regimes for this value of x_0. We find good agreement between the two, especially for smaller values of $E_d = E_b$; for large values of the defect strength,

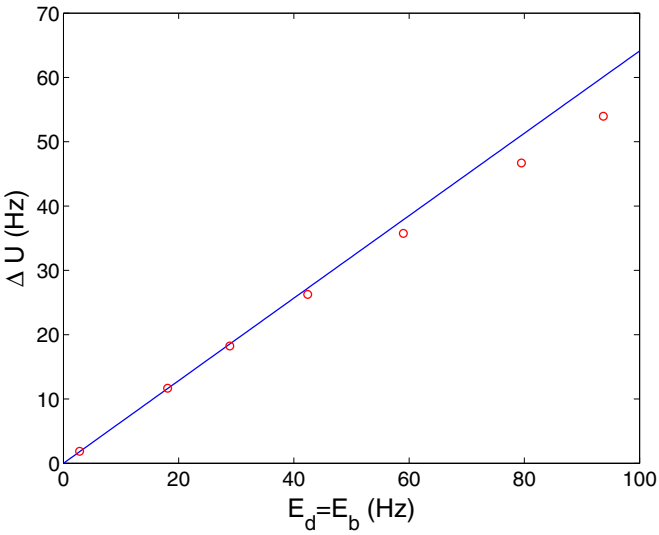

Figure 3. A theoretical comparison of the DB-soliton's potential energy difference ΔU caused by the defect (solid line) with the maximum of the effective barrier height that the DB-soliton particle encounters at the defect, for different values of $E_d = E_b = E$ (red circles). The very good agreement (especially for smaller values E) lends support to the consideration of this case as an example of a classical (solitonic) particle scattering from a barrier.

the perturbative nature of the calculation of equations (8)–(9) may be responsible for the somewhat decreased accuracy in capturing the effective barrier height.

The contour plots of the densities of the dark and bright components corresponding to relatively small and large values of $E > 0$ (corresponding to *IA* and *IB* in figure 2) are illustrated in figure 4 (columns *IA* and *IB*). The top row

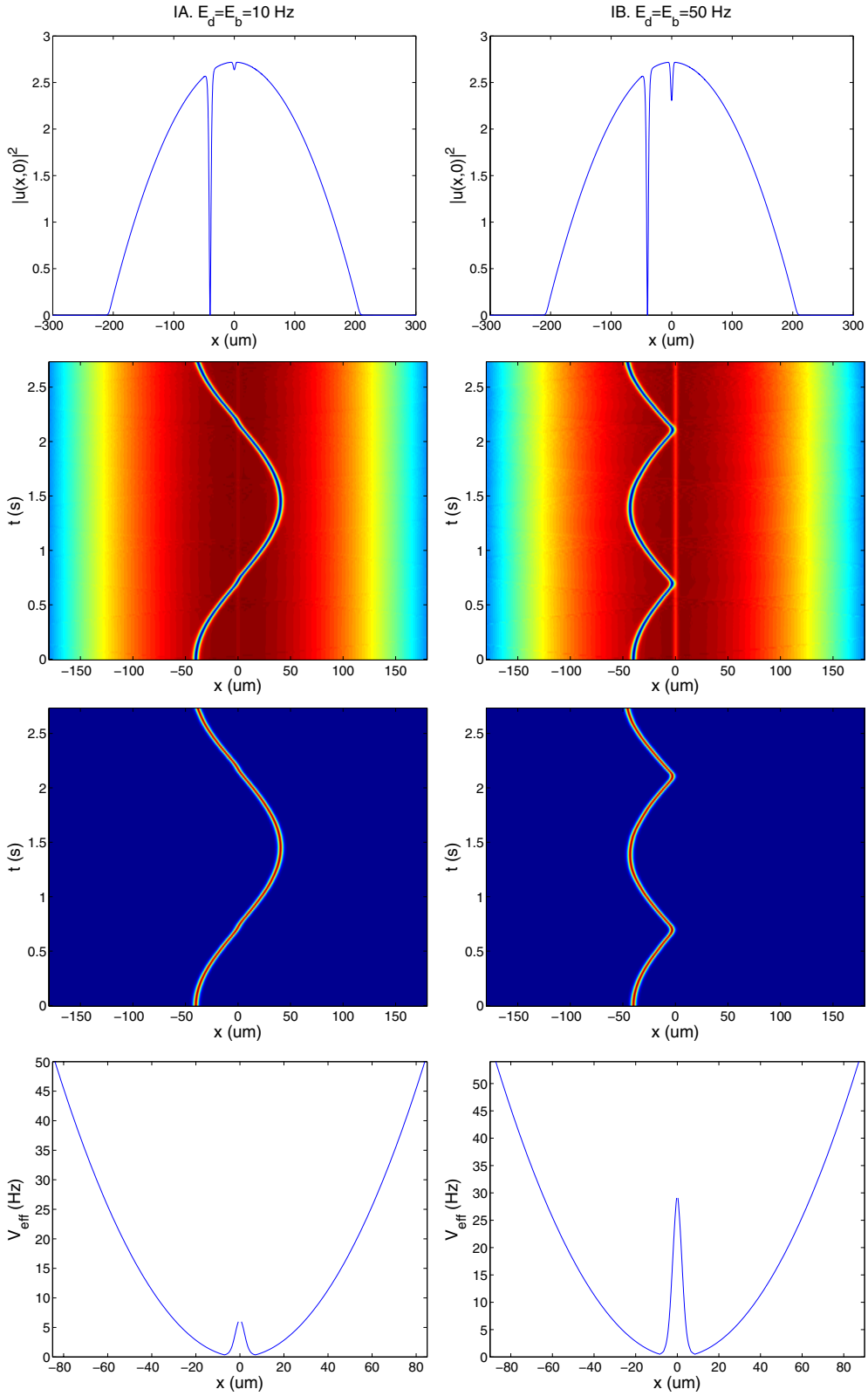

Figure 4. Numerical results for the case of identical repulsive impurities. Top row: initial density profiles of the dark components for a small and large value of $E > 0$. Middle rows: contour plots of the densities of the dark components $|u(x)|^2$ and of the densities of the bright components $|v(x)|^2$. The left panels correspond to a subcritical case, featuring (nearly) full transmission, while the right ones are for a supercritical case with (nearly complete) reflection. Bottom panels: the effective potential encountered by the solitary wave. The low height of the barrier in the left column enables transmission, while its increase in the right panel induces the reflection.

shows the initial density profiles of the corresponding dark components. It is important to highlight here (as it will also become relevant for other cases) that the dark component sustains an increasing density dip as E increases in positive values, while it will correspondingly feature a density bump in the case of increasing negative such values. This is a feature of the ground state in the presence of the defect, as the latter repels for $E > 0$ and attracts for $E < 0$ the atoms in the neighbourhood of $x = 0$. It is clear also by plotting the effective potentials (in the bottom panel of the figure) that the DB faces a weak barrier in case IA and its potential energy is sufficient to overcome it. On the other hand, the barrier is considerably higher in the right panel of case IB, inducing the reflection of the solitary wave.

We complete this section by noting that in the case where both impurities are attractive, i.e. $E_d = E_b = E < 0$, the DB solitons are always transmitted after the collision, for every value of E, hence there is only a transmission regime depicted by blue in figure 2.

3.2. Scattering of DB solitons from an impurity in one component

While the dynamical evolution of the case where the defect acts on both components was found to be fairly straightforward, the case where the barrier is imposed selectively on only one of the components was found to be considerably more complex. We considered both the case where $E_d = 0$ and $E_b \neq 0$ and that where $E_d \neq 0$ and $E_b = 0$. The results show that the following two subcases are equivalent:

(a) $(E_d = 0, E_b > 0) \equiv (E_d < 0,\ E_b = 0)$.
(b) $(E_d = 0, E_b < 0) \equiv (E_d > 0,\ E_b = 0)$.

The case where $E_d = 0$ and $E_b < 0$ represents the existence of an attractive barrier in the bright component and absence of impurity in the dark component. The above equivalence can be most easily qualitatively appreciated in that case (b), hence we present it for that setting. In particular, when an impurity attractively affects the atoms in the bright component, then it favours the 'collection' of atoms near the origin. This, in turn, builds a population of atoms in that neighbourhood which, through the term proportional to g_{12} in the equations of motion, provides a repulsive barrier for the dark component. Hence, the existence of an attractive well solely in the bright component becomes tantamount to having a repulsive barrier in the dark component. An analogous argument can be used to showcase that a repulsive barrier in the bright component, through favouring the absence of atoms in its vicinity, creates an effective well for the dark component atoms. The above feature is directly evident in the diagram of figure 2, hence we only focus on one of the representatives of each of the cases (a) and (b) above.

After the collisions, for $E_d = 0, E_b > 0$, part of the energy is transmitted and part of it is reflected. We denote this as a transmission–reflection regime (coloured green in figure 2). For small values of E_b the DB solitons are mainly transmitted, and when E_b is high enough they are mostly reflected. Equivalent results, when the well depth $|E_d|$ increases, are obtained for the case where $E_d < 0$ and $E_b = 0$, which represents the existence of an attractive well in the dark component and the absence of impurity in the bright one. For small $E_b > 0$, this dynamical behaviour—shown in the left panel of figure 5—can be understood as follows. As discussed above, the repulsion of bright atoms produces an effective attraction of dark atoms, hence inducing an effective potential well, rather than what was anticipated as a potential barrier. It should be noted here that this counter-intuitive effect was quantified in the case of a δ-function potential in [20]. This effect leads to the acceleration of the soliton (with a small back-scatter due to the inelasticity of collision with the defect) visible in the left panels of the figure. To complete the discussion of figure 5, let us briefly touch upon the right panels of the figure. This concerns the case of $E_b < 0$ (while $E_d = 0$, namely case (b) above). The corresponding situation here, when E_b is small presents a repulsive effect for the dark atoms and as such results in an effective barrier. This prediction is also corroborated by the analytical considerations for the δ-function case of [20]. This, in turn, leads to the reflection dynamics observed in the right panels of figure 5. Notice that for very small negative values of E_b, soliton transmission is actually observed, but this regime rapidly changes to the reflection shown in the figure.

We now turn to the case of large barrier strength in figure 6. In this setting, there is a fundamental difference in comparison to the case of weak barrier presented previously. This consists of the fact that for small E_b, the defining characteristic in the DB-soliton and defect interaction is the nature of the potential for the dark component (which, as we saw, was somewhat counter-intuitively the opposite of the one for the bright component). However, for large E_b, the nature of the potential for the bright component becomes important and hence in this case, large positive E_b also induces a locally strong repulsive potential for the bright atoms. On the other hand, large negative E_b creates a large attractive potential for the bright atoms. However, the latter tends to favour the trapping of the atoms of the bright component together with those of the dark component, leading essentially to the formation of a defect mode, alongside a partial reflection of the soliton. These characteristics, namely reflection for E_b large and positive and the possibility of trapping, along with reflection for E_b large and negative, are illustrated in the panels of figure 6.

An example of intermediate values of E_b and their associated dynamics can be found in figure 7. In these examples, for positive E_b, the impurity leads to partial transmission and partial reflection, but does not enable the possibility of trapping at the defect. In this case, the transmitted fraction of the soliton (which is also present in the cases of figures 5 and 6) is so energetic and localized that it can be directly observed; the transmitted soliton has a velocity different from that of the reflected soliton, and consequently, its oscillation frequency differs as well. The possibility of trapping at the defect is explored for $E_b < 0$, whereby there is a fraction of atoms which is trapped at the defect, while also a considerable fraction appears to be reflected; see e.g. the right panel of figure 7. We notice that in the case

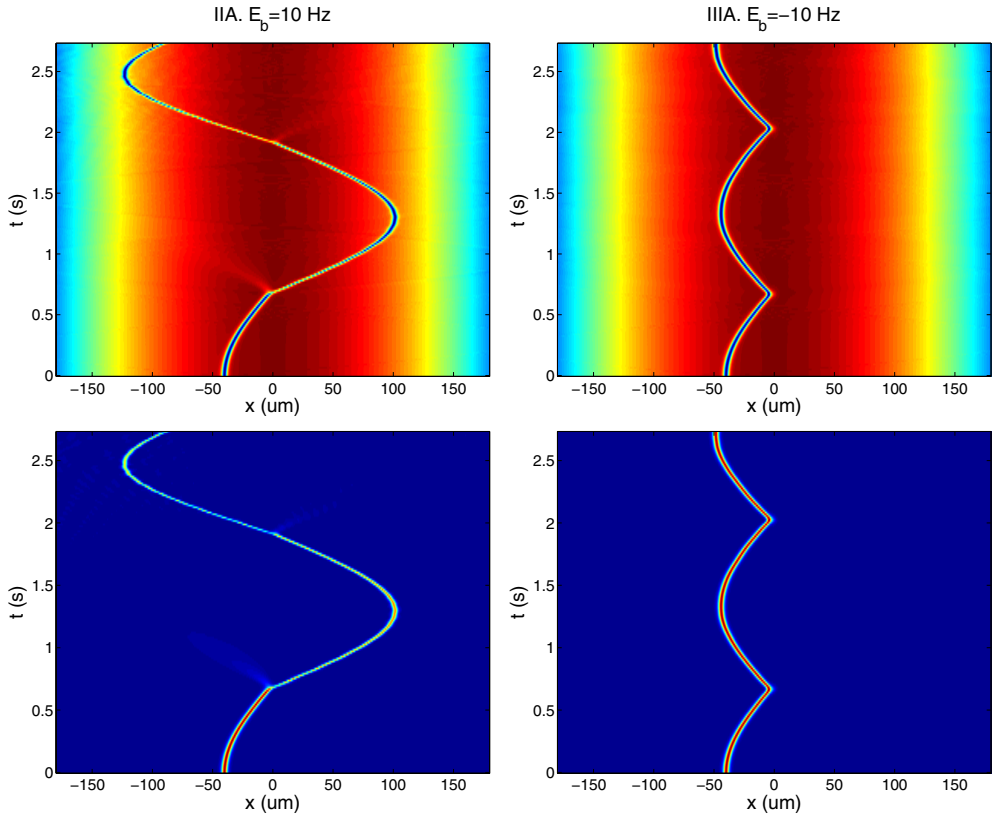

Figure 5. Numerical comparison, for a small value of $|E_b|$, between the case with repulsive bright impurity and the case with attractive bright impurity, with $E_d = 0$. Column IIA: repulsive bright impurity with $E_b = 10$ Hz and $E_d = 0$. Column IIIA: attractive bright impurity with $E_b = -10$ Hz and $E_d = 0$. Top row: the dark components $|u(x,t)|^2$. Bottom row: the bright components $|v(x,t)|^2$.

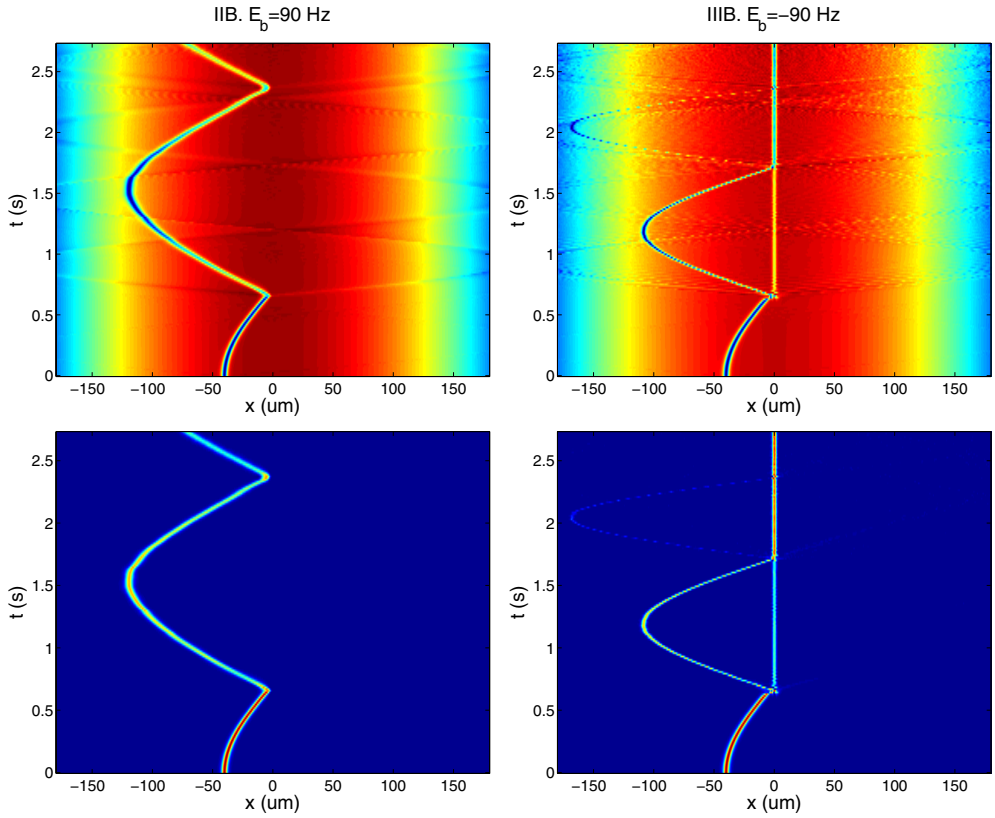

Figure 6. Numerical comparison, for a high value of $|E_b|$, between the case with repulsive bright impurity and the case with attractive bright impurity, with $E_d = 0$. Column IIB: repulsive bright impurity with $E_b = 90$ Hz and $E_d = 0$. Column IIIB: attractive bright impurity with $E_b = -90$ Hz and $E_d = 0$. Top row: the dark components $|u(x,t)|^2$. Bottom row: the bright components $|v(x,t)|^2$.

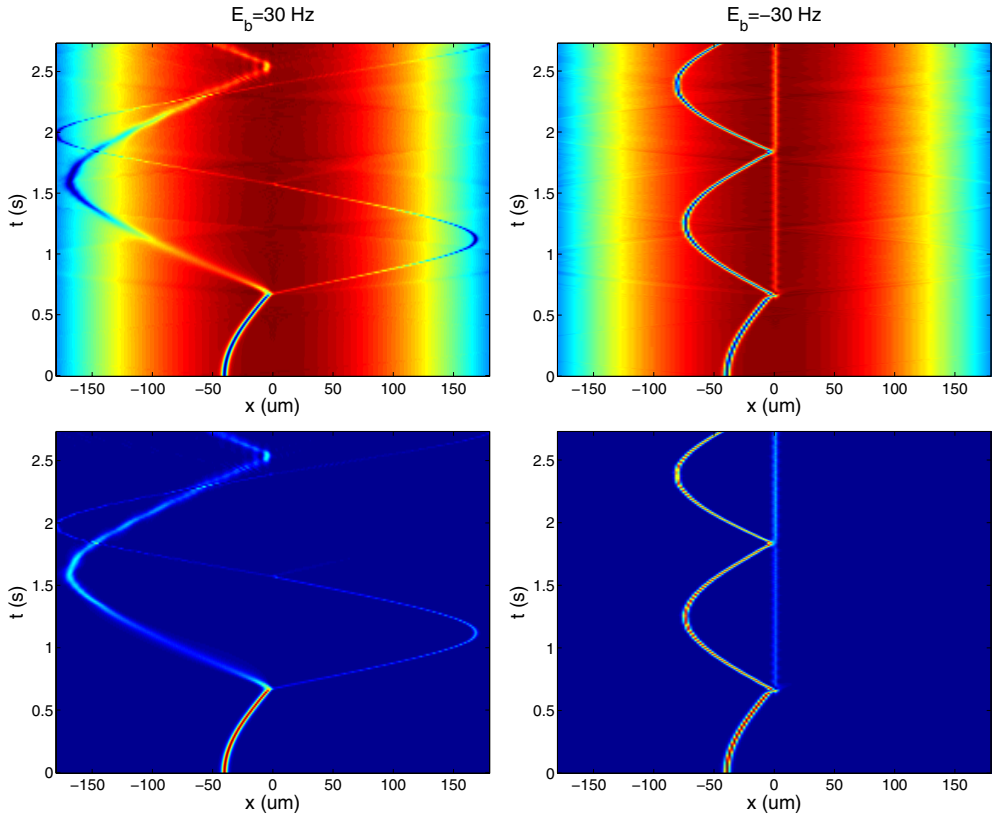

Figure 7. Similar to the previous two figures, but for an intermediate value of $|E_b|$.

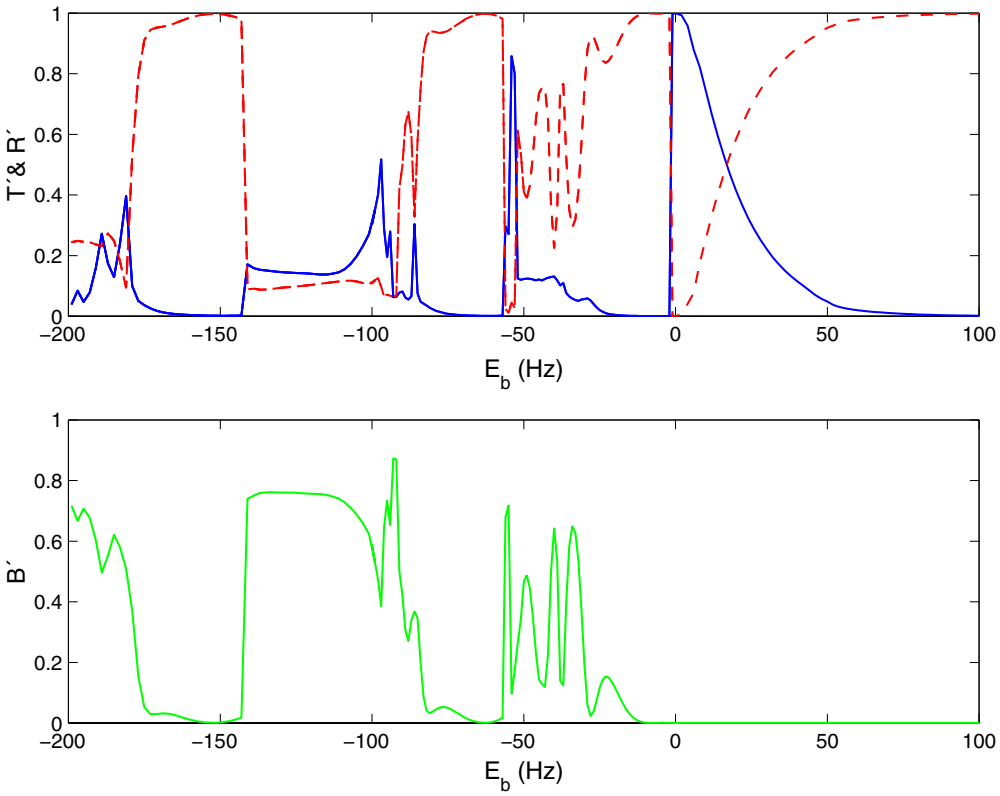

Figure 8. (Top) Numerical representation of T' (full blue line, top panel) and R' (dashed red line, top panel) and B' (full green line, bottom panel) versus E_b for the case $E_d = 0$.

where there is no impurity affecting the dark component and where there exists an attractive well in the bright one, as the well depth $|E_b|$ increases, two regimes appear alternatively: a reflection regime and a trapping–transmission–reflection regime (coloured red and brown, respectively, in region III of figure 2). Indeed, this alternation may be quite complex and a characteristic example thereof is presented in figure 8, where the fractions of atoms transmitted through the defect, reflected from it and trapped in the immediate vicinity of the barrier are measured. These are quantitatively described by the transmission, reflection and trapping coefficients. Notice that the time-dependent coefficients are defined as

$$T(t) = \frac{\int_{\epsilon_b}^{\infty} |v(x,t)|^2 \,\mathrm{d}x}{\int_{-\infty}^{\infty} |v(x,t)|^2 \,\mathrm{d}x},$$
$$R(t) = \frac{\int_{-\infty}^{-\epsilon_b} |v(x,t)|^2 \,\mathrm{d}x}{\int_{-\infty}^{\infty} |v(x,t)|^2 \,\mathrm{d}x},$$
$$B(t) = \frac{\int_{-\epsilon_b}^{\epsilon_b} |v(x,t)|^2 \,\mathrm{d}x}{\int_{-\infty}^{\infty} |v(x,t)|^2 \,\mathrm{d}x}. \qquad (10)$$

Figure 8 depicts these coefficients at time t', namely R', T' and B', with t' being the time where the bright component of the DB soliton reaches its maximum excursion after the first interaction with the defect. The figure illustrates that the full dynamics features more complicated resonant type transmission events, as well as alternating windows of predominantly reflection or predominantly trapping. These complex scenarios are beyond the scope of the particle analysis provided herein. We do note, however, the apparent similarity of these results with the ones obtained in the case of a single component bright soliton which scatters off of a quantum well [42]. In the latter case, the variational analysis was already fairly cumbersome even for a δ-function potential, while here it is rendered more elaborate by the presence of two-components and the Gaussian form of the barrier. A more detailed analysis, perhaps in the simpler δ-function attractive setting based on a two-mode variational ansatz would constitute an interesting problem for further studies. Nevertheless, we should point out that this behaviour is similar to that obtained for the case where there exists a repulsive barrier in the dark component and there is no impurity affecting the bright component.

4. Conclusions and future challenges

In the present work, we have studied the collisions of atomic dark–bright (DB) solitons with narrow defects. Motivated by the potential of experimental studies (a prototypical example of which was shown herein), we considered the setting of a DB soliton impinging on a defect potential. In the case of a bright soliton hitting a well [42, 43] or a barrier [44, 45], this theme has been of intense theoretical and even experimental [52, 53] interest recently. However, far less has been done in the realm of DB solitons.

We have shown that in the case of two equal repulsive barriers acting on both components, the DB solitons demonstrate a clear classical particle behaviour, which involves transmission for weak potentials and reflection for strong ones. Similarly, predominantly transmission type events were observed for equal attractive potentials acting on both components.

On the other hand, we illustrated that more complex scenarios can develop in the case where the impurity acts only on one of the two components. We categorized these cases, illustrating the analogies of a repulsive barrier in the first component with an attractive one in the second component (and vice versa). We explained the low barrier amplitude cases on the basis of somewhat counter-intuitive, cross-component effective potentials and argued that the large amplitude cases may be significantly different due to the role of the defect in both components. We showcased the complexity of the latter by means of cases containing transmission and reflection, or trapping, transmission and reflection together and by monitoring the dependence of the different fractions (of trapping, transmission or reflection), as a function of the barrier amplitude.

It would certainly be interesting to extend this chiefly numerical (but also experimental) study further. On the experimental side, it would be extremely interesting, although more challenging, to engineer potentials that are selective to particular hyperfine states, so that some of the predictions proposed herein could be tested. From a theoretical perspective, it would be very relevant to attempt to distil a simple setting (e.g. a δ-function potential) where a theoretical study of the above reported phenomenology could be appreciated in more quantitative terms. Numerically, it may also be quite significant to appreciate the effect of the width of the barrier, as here we have concentrated on the sign and magnitude (and inter-component interplay of the) barrier. Natural extensions may also concern the possibility of scattering in higher-dimensional settings and evaluation of the role of transverse degrees of freedom therein.

Acknowledgments

PE acknowledges financial support from NSF and ARO. PGK gratefully acknowledges support from NSF-DMS-0806762 and the Alexander von Humboldt Foundation, as well as the Binational Science Foundation. AA, FRR and JC acknowledge financial support from the MICINN project FIS2008-04848. The work of DJF was partially supported by the Special Account for Research Grants of the University of Athens.

References

[1] Pethick C J and Smith H 2002 *Bose–Einstein Condensation in Dilute Gases* (Cambridge: Cambridge University Press)
[2] Pitaevskii L P and Stringari S 2003 *Bose–Einstein Condensation* (Oxford: Oxford University Press)
[3] Kevrekidis P G, Frantzeskakis D J and Carretero-González R 2008 *Emergent Nonlinear Phenomena in Bose–Einstein Condensates: Theory and Experiment* (Heidelberg: Springer)
[4] Carretero-González R, Frantzeskakis D J and Kevrekidis P G 2008 *Nonlinearity* **21** R139
[5] Abdullaev F K, Gammal A, Kamchatnov A M and Tomio L 2005 *Int. J. Mod. Phys.* B **19** 3415
[6] Frantzeskakis D J 2010 *J. Phys. A: Math. Theor.* **43** 213001
[7] Myatt C J, Burt E A, Ghrist R W, Cornell E A and Wieman C E 1997 *Phys. Rev. Lett.* **78** 586

[8] Hall D S, Matthews M R, Ensher J R, Wieman C E and Cornell E A 1998 *Phys. Rev. Lett.* **81** 1539
[9] Khaykovich L, Schreck F, Ferrari G, Bourdel T, Cubizolles J, Carr L D, Castin Y and Salomon C 2002 *Science* **296** 1290
[10] Strecker K E, Partridge G B, Truscott A G and Hulet R G 2002 *Nature* **417** 150
[11] Eiermann B, Anker T, Albiez M, Taglieber M, Treutlein P, Marzlin K-P and Oberthaler M K 2004 *Phys. Rev. Lett.* **92** 230401
[12] Busch T and Anglin J R 2001 *Phys. Rev. Lett.* **87** 010401
[13] Nistazakis H E, Frantzeskakis D J, Kevrekidis P G, Malomed B A and Carretero-González R 2008 *Phys. Rev.* A **77** 033612
[14] Vijayajayanthi M, Kanna T and Lakshmanan M 2008 *Phys. Rev.* A **77** 013820
[15] Rajendran S, Muruganandam P and Lakshmanan M 2009 *J. Phys. B: At. Mol. Opt. Phys.* **42** 145307
[16] Brazhnyi V A and Pérez-García V M 2011 *Chaos Solitons Fractals* **44** 381
[17] Yin C, Berloff N G, Perez-Garcia V M, Brazhnyi V A and Michinel H 2011 *Phys. Rev.* A **83** 051605
[18] Law K J H, Kevrekidis P G and Tuckerman L S 2010 *Phys. Rev. Lett.* **105** 160405
[19] Álvarez A, Cuevas J, Romero F R and Kevrekidis P G 2011 *Physica* D **240** 767
[20] Achilleos V, Kevrekidis P G, Rothos V M and Frantzeskakis D J 2011 *Phys. Rev.* A **84** 053626
[21] Achilleos V, Yan D, Kevrekidis P G and Frantzeskakis D J 2012 *New J. Phys.* **14** 055006
[22] Becker C, Stellmer S, Soltan-Panahi P, Dörscher S, Baumert M, Richter E-M, Kronjäger J, Bongs K and Sengstock K 2008 *Nature Phys.* **4** 496
[23] Hamner C, Chang J J, Engels P and Hoefer M A 2011 *Phys. Rev. Lett.* **106** 065302
[24] Middelkamp S, Chang J J, Hamner C, Carretero-González R, Kevrekidis P G, Achilleos V, Frantzeskakis D J, Schmelcher P and Engels P 2011 *Phys. Lett.* A **375** 642
[25] Yan D, Chang J J, Hamner C, Kevrekidis P G, Engels P, Achilleos V, Frantzeskakis D J, Carretero-González R and Schmelcher P 2011 *Phys. Rev.* A **84** 053630
[26] Hoefer M A, Chang J J, Hamner C and Engels P 2011 *Phys. Rev.* A **84** 041605
[27] Yan D, Chang J J, Hamner C, Hoefer M A, Kevrekidis P G, Engels P, Achilleos V, Frantzeskakis D J and Cuevas J 2012 *J. Phys. B: At. Mol. Opt. Phys.* **45** 115301
[28] Kivshar Y S and Agrawal G P 2003 *Optical Solitons: From Fibers to Photonic Crystals* (San Diego, CA: Academic)
[29] Chen Z, Segev M, Coskun T H, Christodoulides D N, Kivshar Y S and Afanasjev V V 1996 *Opt. Lett.* **21** 1821
[30] Ostrovskaya E A, Kivshar Y S, Chen Z and Segev M 1999 *Opt. Lett.* **24** 327
[31] Chen Z, Segev M, Coskun T H, Christodoulides D N and Kivshar Y S 1997 *J. Opt. Soc. Am.* B **14** 3066–77
[32] Kivshar Y S and Malomed B A 1989 *Rev. Mod. Phys.* **61** 763
[33] Lifshitz I M and Kosevich A M 1966 *Rep. Prog. Phys.* **29** 217
[34] Kosevich A M 1990 *Physica* D **41** 253
[35] Cao X D and Malomed B A 1995 *Phys. Lett.* A **206** 177
[36] Goodman R H, Holmes P J and Weinstein M I 2004 *Physica* D **192** 215
[37] Holmer J, Marzuola J and Zworski M 2007 *Commun. Math. Phys.* **274** 187
Holmer J, Marzuola J and Zworski M 2007 *J. Nonlinear Sci.* **17** 349
[38] Konotop V V, Pérez-García V M, Tang Y-F and Vázquez L 1997 *Phys. Lett.* A **236** 314
[39] Frantzeskakis D J, Theocharis G, Diakonos F K, Schmelcher P and Kivshar Yu S 2002 *Phys. Rev.* A **66** 053608
[40] Bilas N and Pavloff N 2005 *Phys. Rev.* A **72** 033618
[41] Herring G, Kevrekidis P G, Carretero-González R, Malomed B A, Frantzeskakis D J and Bishop A R 2005 *Phys. Lett.* A **345** 144
[42] Ernst T and Brand J 2010 *Phys. Rev.* A **81** 033614
[43] Lee C and Brand J 2006 *Europhys. Lett.* **73** 321
[44] Helm J L, Billam T P and Gardiner S A 2012 *Phys. Rev.* A **85** 053621
[45] Martin A D and Ruostekoski J 2012 *New J. Phys.* **14** 043040
[46] Streltsov A I, Alon O E and Cederbaum L S 2009 *Phys. Rev.* A **80** 043616
[47] Weiss C and Castin Y 2012 *J. Phys. A: Math. Theor.* **45** 455306
[48] Lewenstein M and Malomed B A 2009 *New J. Phys.* **11** 113014
[49] Hansen S D, Nygaard N and Mølmer K 2012 arXiv:1210.1681
[50] Engels P and Atherton C 2007 *Phys. Rev. Lett.* **99** 160405
[51] Dries D, Pollack S E, Hitchcock J M and Hulet R G 2010 *Phys. Rev.* A **82** 033603
[52] Dyke P, Lei S and Hulet R G 2012 Book of abstracts *23rd Int. Conf. on Atomic Physics (Palaiseau, France, 23–27 July)* p 174; see also Cuevas J, Kevrekidis P G, Malomed B A, Dyke P and Hulet R G arXiv:1301.3959
[53] Marchant A L, Wiles T P, Händel S, Yu M M H, Hopkins S A and Cornish S L 2012 Poster presentation *23rd Int. Conf. on Atomic Physics (Palaiseau, France, 23–27 July)*; see also Marchant A L, Billam T P, Wiles T P, Yu M M H, Gardiner S A and Coinish S L arXiv:1301.5759
[54] Manakov S V 1973 *Zh. Eksp. Teor. Fiz.* **65** 505
Manakov S V 1974 *Sov. Phys.—JETP* **38** 248